

Effect of Electromagnetic Pulse Transverse Inhomogeneity on the Ion Acceleration by Radiation Pressure

K. V. Lezhnin,¹ F. F. Kamenets,¹ V. S. Beskin,^{1,2} M. Kando,³ T. Zh. Esirkepov,³ and S. V. Bulanov^{1,3,*}

¹*Moscow Institute of Physics and Technology, Institutskiy per. 9, Dolgoprudny, Moscow Region, 141700, Russia*

²*Russian Acad. Sci., P. N. Lebedev Phys. Inst., Leninskii Prospekt 53, Moscow 119991, Russia*

³*Japan Atomic Energy Agency, Kansai Photon Science Institute,
8-1-7 Umemidai, Kizugawa-shi, Kyoto, 619-0215 Japan*

(Dated: December 30, 2014)

In the ion acceleration by radiation pressure a transverse inhomogeneity of the electromagnetic pulse results in the displacement of the irradiated target in the off-axis direction limiting achievable ion energy. This effect is described analytically within the framework of the thin foil target model and with the particle-in-cell simulations showing that the maximum energy of accelerated ions decreases while the displacement from the axis of the target initial position increases. The results obtained can be applied for optimization of the ion acceleration by the laser radiation pressure with the mass limited targets.

Keywords: Relativistic laser plasmas, Ion acceleration, Radiation pressure

PACS numbers: 52.38.Kd, 52.65.Rr

INTRODUCTION

Studies of the high energy ion generation in the interaction between an ultraintense laser pulse and a small overdense targets, are of fundamental importance for various research fields ranging from the developing the ion sources for thermonuclear fusion and medical applications to the investigation of high energy density phenomena in relativistic astrophysics (see review articles [1–7] and the literature cited therein).

Theory and experiments on laser acceleration can clarify the basic features of particle acceleration in astrophysical objects. Indeed, according to common point of view, activity of radio pulsars, active galactic nuclei, and even gamma-bursts connects with the highly magnetized wind in which electric field is approximately equal to magnetic one [8]. Charged particles produced in such a wind can get the energy of the order of $m_\alpha c^2 \gamma_w^2$ that is much higher than the energy of the wind ($\approx mc^2 \gamma_w$) [9, 10]. Here γ_w is the Lorentz-factor associated with the wind velocity. Moreover, interacting with the external environment (the companion star in a close binary system, the current sheets in the pulsar wind), a region where the electric field is greater than the magnetic can form where therefore the acceleration of particles can be even more effective [12].

Depending on the laser and target parameters different regimes of acceleration appear – from acceleration at the target surface called the Target Normal Sheath Acceleration (TNSA) [13, 15, 16] through the Coulomb explosion [17–20] to radiation pressure dominance acceleration (RPDA) regime [21–24]. The ion acceleration regimes are shown in the plane of the laser intensity – the surface density $n_e l_0$ of the target in Fig. 1 (see also [6]). Here n_e is the electron density in the target and l_0

is its thickness. At the intensity above 10^{18} W/cm^2 the plasma electron energy becomes relativistic. The dashed line, is given by the formula

$$a_0 = n_e r_e \lambda l_0, \quad (1)$$

where $a_0 = eE_0/m_e \omega c$ is the normalized laser pulse amplitude, ω and $\lambda = 2\pi c/\omega$ are the laser frequency and wavelength, respectively, and $r_e = e^2/m_e c^2 = 2.8 \times 10^{-13} \text{ cm}$ is the classical electron radius; m_e and e are the electron mass and charge, and c is the speed of light in vacuum. This line separates the intensity – surface density plane into two domains. In the domain below the line the plasma is opaque and above it is transparent for the laser radiation [25]. When the laser radiation interacts with the opaque target a relatively small portion of hot electrons can escape forming a sheath with strong electric charge separation electric field where the acceleration occurs in the TNSA regime. Above the dashed line the laser radiation is so intense that it blows out almost all electrons from the target irradiated region. The remaining ions undergo fast expansion, the Coulomb explosion, due repelling of noncompensated electric charges. At the opaqueness-transparency threshold, in the vicinity of the dashed line in Fig. 1 the optimal conditions for the ion acceleration in the RPDA regime are realized [22, 27]. A fundamental feature of the RPDA acceleration process, proposed by Veksler [21], is its high efficiency, as the ion energy per nucleon turns out to be proportional in the ultrarelativistic limit to the electromagnetic pulse energy. As far it concerns the experimental evidence of the RPDA mechanism there are indications on its realization in the laser thin foil interaction reported in Refs. [29–31].

The usage of a finite transverse size target, it is called the Mass Limited Target (MLT) or the Reduced Mass

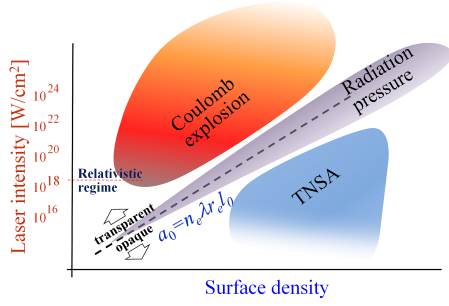


FIG. 1. The ion acceleration regimes in the plane of the laser intensity $[\text{W}/\text{cm}^2]$ –the surface density $n_e l_0$ of the target.

Target [32–38], including the cluster targets [18, 39], provide a way for enhancement of the ion energy and acceleration efficiency and a way for high brightness X-ray generation [40]. The irradiation of MLT by enough high intensity lasers is one of the most perspective approaches to develop compact ion accelerators [28, 41].

In the present paper, we discuss the RPDA regime under the conditions when a transverse inhomogeneous laser pulse irradiates a MLT positioned not precisely at the laser pulse axis. This situation naturally occurs due to a finite pointing stability of the laser systems. As a result the transverse component of the radiation pressure leads to the displacement of the irradiated target in the off-axis direction. Apparently, after a finite interval of time the target leaves the laser pulse preventing from the further ion acceleration. Below on the ground of a theoretical model of relativistic mirror [22, 28, 41] we calculate the acceleration time and hence the achieved ion energy dependence on the laser pulse amplitude and transverse size and on the initial displacement of the target from the laser axis. According to recently published papers, various instabilities of the target plasma appear in the RPDA regime, for instance, the Rayleigh-Taylor-like instability [43] leads to the target modulation forming the low density bubbles and high density clumps resulting in the broadening of the accelerated ion energy spectrum. In order to elucidate the kinetic, nonlinear and instability effects we carry out the PIC simulations of the finite waist laser pulse interaction with the MLT by using the REMP code [44].

DYNAMICS OF THE MASS LIMITED TARGET POSITIONED SLIGHTLY OFF-AXIS

The Equations of Motion

We describe the nonlinear dynamics of a laser accelerated target within the framework of the thin shell approximation formulated by Ott [45] and further generalized on the 3D geometry in Refs. [46, 47] and extended to the relativistic case in Refs. [41, 43].

In a way of Refs. [41–43] here we derive of the motion equations required for further consideration of the MLT dynamics. The equations of motion of the surface element of a thin foil target in the laboratory frame of reference can be written in the form

$$\frac{d\mathbf{p}}{dt} = \frac{\mathcal{P}\nu}{\sigma}, \quad (2)$$

where \mathbf{p} , \mathcal{P} , ν , and σ are the momentum, light pressure, unit vector normal to the shell surface element, and surface density, $\sigma = n l_0$, respectively. Here n and l are the plasma ion density and shell thickness. We determine the surface element Δs as carrying $\Delta N = \sigma \Delta s$ particles, with ΔN constant in time. We take the shell initially to be at rest, at $t = 0$, in the plane $x = 0$. In order to describe how its shape and position change with time it is convenient to introduce the Lagrange coordinates η and ζ playing the role of the markers of the shell surface element. The shell shape and position are given by the equation

$$\mathbf{M} = \mathbf{M}(\eta, \zeta, t) \equiv \{x(\eta, \zeta, t), y(\eta, \zeta, t), z(\eta, \zeta, t)\}. \quad (3)$$

At a regular point, the surface area of a shell element and the unit vector normal to the shell are equal to

$$\nu \Delta s = \partial_\eta \mathbf{M} \times \partial_\zeta \mathbf{M} d\eta d\zeta \quad (4)$$

and

$$\nu = \frac{\partial_\eta \mathbf{M} \times \partial_\zeta \mathbf{M}}{|\partial_\eta \mathbf{M} \times \partial_\zeta \mathbf{M}|}, \quad (5)$$

respectively (see e.g., [48]). The particle number conservation implies $\sigma \Delta s = \sigma_0 \Delta s_0$, where $\sigma_0 = n_0 l_0$. This yields

$$\sigma = \frac{\sigma_0}{|\partial_\eta \mathbf{M} \times \partial_\zeta \mathbf{M}|}. \quad (6)$$

Using these relationships and representing the coordinates x_i as

$$x = \xi_x(\eta, \zeta, t), \quad (7)$$

$$y = \eta + \xi_y(\eta, \zeta, t), \quad (8)$$

$$z = \zeta + \xi_z(\eta, \zeta, t) \quad (9)$$

with initial conditions: $\xi_i(\eta, \zeta, 0) = 0$ and $\dot{\xi}_i(\eta, \zeta, 0) = v_i(\eta, \zeta, 0)$, we obtain the equations of motion in the form [49]

$$\sigma_0 \partial_t p_x = \mathcal{P} (1 + \partial_\eta \xi_y + \partial_\zeta \xi_z + \{\xi_y, \xi_z\}), \quad (10)$$

$$\sigma_0 \partial_t p_y = \mathcal{P} (-\partial_\eta \xi_x + \{\xi_z, \xi_x\}), \quad (11)$$

$$\sigma_0 \partial_t p_z = \mathcal{P} (-\partial_\zeta \xi_x + \{\xi_x, \xi_y\}), \quad (12)$$

$$\partial_t \xi_i = c \frac{p_i}{(m_\alpha^2 c^2 + p_k p_k)^{1/2}}, \quad (13)$$

Here m_α is the ion mass, $i = 1, 2, 3$, and summation over repeated indices is assumed,

$$\{\xi_j, \xi_k\} = \partial_\eta \xi_j \partial_\zeta \xi_k - \partial_\zeta \xi_j \partial_\eta \xi_k \quad (14)$$

are Poisson's brackets. This form of the equations is particularly convenient for analysing small but finite displacement of the target elements from the axis.

The radiation pressure on the shell exerted by a circularly polarized electromagnetic wave propagating along the x -axis with amplitude $E = E(t - x/c)$ is

$$\mathcal{P} = K \frac{E^2}{4\pi} \left(\frac{1 - \beta_x}{1 + \beta_x} \right), \quad (15)$$

where $\beta_x = p_x(m_\alpha^2 c^2 + p_x^2)^{-1/2}$ is the shell normalized velocity in the x -direction. The coefficient K equal to

$$K = 2|\rho|^2 + |\alpha|^2 \quad (16)$$

depends on $|\rho|^2$ and $|\alpha|^2$ which are the light reflection and absorption coefficients, respectively (see also Ref. [50]). Effects of the reflection coefficient dependence on the ion energy due to the relativistic transparency has been discussed in Refs. [27, 51]. Below we shall not consider the relativistic transparency effects assuming ideally reflecting light target with $K = 2$.

We note here that in Eqs. (10–12) there is no a force acting between the target surface elements, i. e. we can consider a finite transverse size MLT for which the Lagrange coordinates η and ζ belong to a finite domain: $\eta \in [\eta_1, \eta_2]$ and $\zeta \in [\zeta_1, \zeta_2]$.

For homogeneous laser pulse, $E = \text{constant}$, the flat MLT is accelerated along the x -axis with $p_y = 0$, $p_z = 0$, $\xi_y = 0$, and $\xi_z = 0$. The ion momentum and displacement in the x -direction are given by dependences on time [22]:

$$p_x^{(0)}(t) = m_\alpha c \left(\frac{t}{t_{1/3}} \right)^{1/3}, \quad (17)$$

$$\xi_x^{(0)}(t) = ct - 3ct_{1/3}^{2/3} t^{1/3}, \quad (18)$$

where the characteristic time is

$$t_{1/3} = \frac{8\pi\sigma_0 m_\alpha c}{3E^2}. \quad (19)$$

Here we have assumed that the target energy is ultrarelativistic, $p_x^{(0)}/m_\alpha c \gg 1$.

Using relationships (17) and (18) we can easily find that the finite duration, t_{las} , laser pulse accelerates the ions up to the energy $\mathcal{E} = m_\alpha c^2 \gamma_{max}$ with the gamma-factor given by

$$\gamma_{max} = \frac{E^2 t_{las}}{4\pi\sigma_0 m_\alpha c}. \quad (20)$$

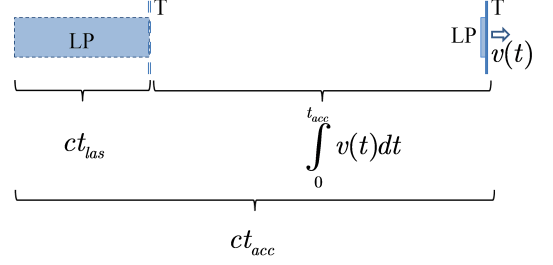


FIG. 2. Laser pulse LP and the target T at $t = 0$ and $t = t_{acc}$

According to Eq. (17) the acceleration time, t_{acc} , can be defined via $\gamma_{max} = (t_{acc}/t_{1/3})^{1/3}$. We find it taking into account that the laser pulse rear reaches the target at $t = t_{acc}$, as it is illustrated in Fig. 2. The acceleration time is determined by equation

$$t_{las} = \int_0^{t_{acc}} \left(1 - \frac{v(t)}{c} \right) dt \approx \frac{1}{2} \int_0^{t_{acc}} \frac{dt}{\gamma(t)^2} \quad (21)$$

This and Eq. (20) yield

$$t_{acc} = \frac{2}{3} \gamma_{max}^2 t_{las}. \quad (22)$$

The Mass Limited Target Irradiated by Gaussian Laser Pulse

In order to analyse the transverse motion of the MLT irradiated by the laser pulse we consider the pulse whose envelope has a Gaussian form,

$$E(y, z) = E_0 \exp \left(-\frac{y^2}{2l_y^2} - \frac{z^2}{2l_z^2} \right) \quad (23)$$

with the laser pulse width equal to l_y and l_z in the y - and z -direction, respectively.

Assuming a smallness of the transverse displacement, $\xi_y \ll \eta$, $\xi_z \ll \zeta$, and considering the near-axis region, $\eta \ll l_y$, $\zeta \ll l_z$, we obtain from Eqs. (10–12) the linearized system of equations,

$$\begin{aligned} \partial_t \left((\gamma^{(0)}(t))^3 \partial_t \xi_x^{(1)} \right) = \\ \frac{c}{(\gamma^{(0)}(t))^2 t_{1/3}^{(0)}} \left(\partial_\eta \xi_y^{(1)} + \partial_\zeta \xi_z^{(1)} - \frac{\eta^2}{l_y^2} - \frac{\zeta^2}{l_z^2} \right), \end{aligned} \quad (24)$$

$$\partial_t \left(\gamma^{(0)}(t) \partial_t \xi_y^{(1)} \right) = -\frac{c}{(\gamma^{(0)}(t))^2 t_{1/3}^{(0)}} \partial_\eta \xi_x^{(1)}, \quad (25)$$

$$\partial_t \left(\gamma^{(0)}(t) \partial_t \xi_z^{(1)} \right) = -\frac{c}{(\gamma^{(0)}(t))^2 t_{1/3}^{(0)}} \partial_\zeta \xi_x^{(1)} \quad (26)$$

with given dependence on time of the ion gamma-factor

$$\gamma^{(0)}(t) = \left(\frac{t}{t_{1/3}^{(0)}} \right)^{1/3}, \quad (27)$$

which is found within the framework of the 1D model of the RPDA thin foil acceleration [22]. The approach used corresponds to so-called betatron approximation well known in the theory of standard accelerators of charged particles [52]. In these expressions the characteristic time is $t_{1/3}^{(0)} = 8\pi\sigma_0 m_\alpha c / 3E_0^2$.

In order to find the solution to the system of equations in partial derivatives (24–26) we use the ansatz

$$\xi_x^{(1)}(\eta, \zeta, t) = \Xi_x(t) + \Xi_{x\eta\eta}(t)\eta^2 + \Xi_{x\zeta\zeta}(t)\zeta^2, \quad (28)$$

$$\xi_y^{(1)}(\eta, \zeta, t) = \Xi_{y\eta}(t)\eta, \quad (29)$$

$$\xi_z^{(1)}(\eta, \zeta, t) = \Xi_{z\zeta}(t)\zeta, \quad (30)$$

which is a self-similar solution reducing Eqs. (24–26) to ordinary differential equations for the functions $\Xi_x(t)$, $\Xi_{x\eta\eta}(t)$, $\Xi_{x\zeta\zeta}(t)$, $\Xi_{y\eta}(t)$, and $\Xi_{z\zeta}(t)$:

$$\frac{d}{d\tau} \left(\gamma^{(0)} \frac{d\Xi_{x\eta\eta}}{d\tau} \right) = -\frac{1}{l_y^2}, \quad (31)$$

$$\frac{d}{d\tau} \left(\gamma^{(0)} \frac{d\Xi_{x\zeta\zeta}}{d\tau} \right) = -\frac{1}{l_z^2}, \quad (32)$$

$$\frac{d}{d\tau} \left(\frac{1}{\gamma^{(0)}} \frac{d\Xi_{y\eta}}{d\tau} \right) = -2\Xi_{x\eta\eta}, \quad (33)$$

$$\frac{d}{d\tau} \left(\frac{1}{\gamma^{(0)}} \frac{d\Xi_{z\zeta}}{d\tau} \right) = -2\Xi_{x\zeta\zeta}, \quad (34)$$

$$\frac{d}{d\tau} \left(\gamma^{(0)} \frac{d\Xi_x}{d\tau} \right) = \Xi_{y\zeta} + \Xi_{z\zeta}. \quad (35)$$

We introduced a new independent variable equal to

$$\tau = \left(\frac{c}{t_{1/3}^{(0)}} \right)^{1/2} \int_0^t \frac{dt}{(\gamma^{(0)}(t))^2} \approx 3c^{1/2} (t_{1/3}^{(0)})^{1/6} t^{1/3}. \quad (36)$$

For initial conditions $\xi_x^{(1)}(\eta, \zeta, 0) = 0$ and $\dot{\xi}_x^{(1)}(\eta, \zeta, 0) = 0$, solution to Eqs. (31–35) reads

$$\Xi_{x\eta\eta} = -\frac{9ct}{l_y^2} \left(\frac{t_{1/3}}{t} \right)^{2/3}, \quad \Xi_{x\zeta\zeta} = -\frac{9ct}{l_z^2} \left(\frac{t_{1/3}}{t} \right)^{2/3}, \quad (37)$$

$$\Xi_{y\eta} = \frac{81(ct)^2}{4l_y^2} \left(\frac{t_{1/3}}{t} \right)^{2/3}, \quad \Xi_{z\zeta} = \frac{81(ct)^2}{4l_z^2} \left(\frac{t_{1/3}}{t} \right)^{2/3}, \quad (38)$$

$$\Xi_x = -\frac{729(ct)^3}{100} \left(\frac{t_{1/3}}{t} \right)^{4/3} \left(\frac{1}{l_y^2} + \frac{1}{l_z^2} \right). \quad (39)$$

As it is seen from Eqs. (29) and (38) the target element with initial coordinates η and ζ moves in the transverse direction with the displacement proportional to $t^{4/3}$. We can estimate the time required to leave the region with strong laser field as

$$\delta t_\perp = \left(\frac{4l_\perp^3}{81\delta r_0} \right)^{3/4} \frac{1}{c^{3/2} t_{1/3}^{1/2}} \quad (40)$$

with $l_\perp = \min\{l_y, l_z\}$ and $\delta r_0 = \max\{\eta, \zeta\}$. According to Eqs. (20) and (40) the achieved ion energy is of the order of

$$\mathcal{E}_\alpha = m_\alpha c^2 \left(\frac{\delta t_\perp}{t_{1/3}} \right)^{1/3}, \quad (41)$$

which implies $\delta t_\perp < t_{acc}$. The opposite case realized for small enough initial position of the MLT centroid, δr_0 , and/or wide enough laser pulse corresponds to the perfect laser-target alignment.

Using obtained above relationships we can write the characteristic time $t_{1/3}$ as

$$t_{1/3} = \frac{2\omega_{pe}^2}{\omega^2} \frac{m_\alpha}{m_e} \frac{l_0}{c} \frac{1}{a_0^2}, \quad (42)$$

which for the solid density target, $\omega_{pe}^2/\omega^2 \approx 10^2$, of the thickness $l_0 = 0.1\mu\text{m}$ for the laser intensity of the order of $10^{23}\text{W}/\text{cm}^2$ corresponding to $a_0 = 300$, $m_\alpha = m_p$, yields $t_{1/3} \approx 1.5\text{fs}$. In the case of perfect laser-target alignment the maximal achievable ion (proton) energy $m_\alpha c^2(t_{las}/3t_{1/3})$ for 100 fs laser pulse duration is about 20 GeV with the acceleration time given by Eq. (22) equal to 10 ps. The perfect alignment condition implies $t_\perp > t_{acc}$.

Super Gaussian Laser Pulse Interaction with Mass Limited Target

Here we analyse the case when the laser pulse when its envelope has Super-Gaussian form,

$$E(y, z) = E_0 \exp \left(-\frac{y^4}{2l_y^4} \right), \quad (43)$$

with the index equal to 4. For the sake of brevity we consider two-dimensional geometry. Generalization to the 3D case is straightforward.

For small transverse displacement, $\xi_y \ll \eta$, in the near-axis region, $\eta \ll l_y$, within the framework of the betatron approximation the target dynamics is described by the linearized system of equations,

$$\partial_\tau \left(\gamma^{(0)} \partial_\tau \xi_x^{(1)} \right) = \partial_\eta \xi_y^{(1)} - \frac{\eta^4}{l_y^4}, \quad (44)$$

$$\partial_\tau \left(\frac{1}{\gamma^{(0)}} \partial_\tau \xi_y^{(1)} \right) = \partial_\eta \xi_x^{(1)} \quad (45)$$

with the independent variable τ defined by Eq. (36) and the ion gamma-factor $\gamma^{(0)}$ given by Eq. (27).

The self-similar solution to Eqs. (44–45) has a form

$$\xi_x^{(1)}(\eta, \tau) = \Xi_x(\tau) + \Xi_{x\eta\eta}(\tau)\eta^2 + \Xi_{x\eta\eta\eta\eta}(\tau)\eta^4, \quad (46)$$

$$\xi_y^{(1)}(\eta, \tau) = \Xi_{y\eta}(\tau)\eta + \Xi_{y\eta\eta\eta}(\tau)\eta^3. \quad (47)$$

Substituting these functions to Eqs. (44–45) we obtain ordinary differential equations:

$$\frac{d}{d\tau} \left(\gamma^{(0)} \frac{d\Xi_{x\eta\eta\eta\eta}}{d\tau} \right) = -\frac{1}{l_y^4}, \quad (48)$$

$$\frac{d}{d\tau} \left(\frac{1}{\gamma^{(0)}} \frac{d\Xi_{y\eta\eta\eta}}{d\tau} \right) = -4\Xi_{x\eta\eta\eta\eta}, \quad (49)$$

$$\frac{d}{d\tau} \left(\gamma^{(0)} \frac{d\Xi_{x\eta\eta}}{d\tau} \right) = 3\Xi_{y\eta\eta\eta}, \quad (50)$$

$$\frac{d}{d\tau} \left(\frac{1}{\gamma^{(0)}} \frac{d\Xi_{y\eta}}{d\tau} \right) = -2\Xi_{x\eta\eta}, \quad (51)$$

$$\frac{d}{d\tau} \left(\gamma^{(0)} \frac{d\Xi_x}{d\tau} \right) = \Xi_{y\eta}. \quad (52)$$

For zero initial conditions for the displacement $\xi_i^{(1)}(\eta, 0) = 0$ and its time derivative $\dot{\xi}_i^{(1)}(\eta, 0) = 0$, solution to Eqs. (48–52) reads

$$\Xi_{x\eta\eta\eta\eta} = -\frac{9ct}{l_y^4} \left(\frac{t_{1/3}}{t} \right)^{2/3}, \quad \Xi_{y\eta\eta\eta} = \frac{81(ct)^2}{2l_y^4} \left(\frac{t_{1/3}}{t} \right)^{2/3}, \quad (53)$$

$$\Xi_{x\eta\eta} = \frac{4374(ct)^3}{100l_y^4} \left(\frac{t_{1/3}}{t} \right)^{4/3}, \quad \Xi_{y\eta} = -\frac{6561(ct)^4}{400l_y^4} \left(\frac{t_{1/3}}{t} \right)^{4/3}, \quad (54)$$

$$\Xi_x = -\frac{285768(ct)^5}{156800l_y^4} \left(\frac{t_{1/3}}{t} \right)^2. \quad (55)$$

As it follows from expressions (44–45) and (53–55) the target is deformed in such the way that the periphery expands and the near-axis region contracts. This paradoxical behaviour can be explained by the fact that due to the density decreasing in the peripheral regions the target elements there move forward faster modulating the foil curvature, which results in contraction of the near-axis elements, which is distinctly seen in Fig. 3. The longitudinal, along the x -axis velocity has two maxima, the transverse, y -component velocity gradient is positive at large y , which corresponds to the foil expansion, and it is negative near the axis corresponding to the foil compression.

RESULTS OF PARTICLE-IN-CELL SIMULATIONS

Theoretical analysis of the target off-axis displacement effects has been carried within the framework of the linearized model equations (24–26). In order to take into account the nonlinear and kinetic effects, the target deformation and instability we have conducted a series of 2D-PIC simulations using the two-dimensional version of relativistic electromagnetic code REMP [44].

The simulation box is $300\lambda \times 100\lambda$ with mesh resolution of 20 cells per wavelength. The total number of particles

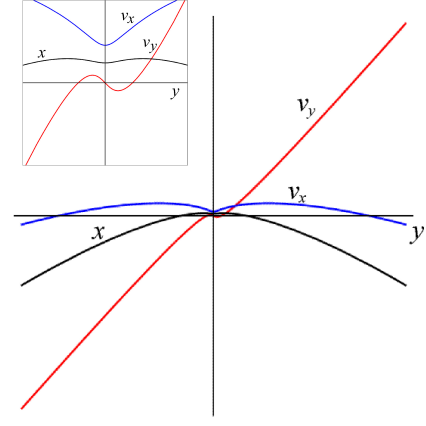


FIG. 3. Thin target deformation by the super-Gaussian laser pulse. The curves x , v_x and v_y show the target position and x - and y -components of the target element velocity in the x, y -plane for $l_y/ct_{1/3} = 2$ at $t/t_{1/3} = 0.5$. Inset: close-up of the near-axis region.

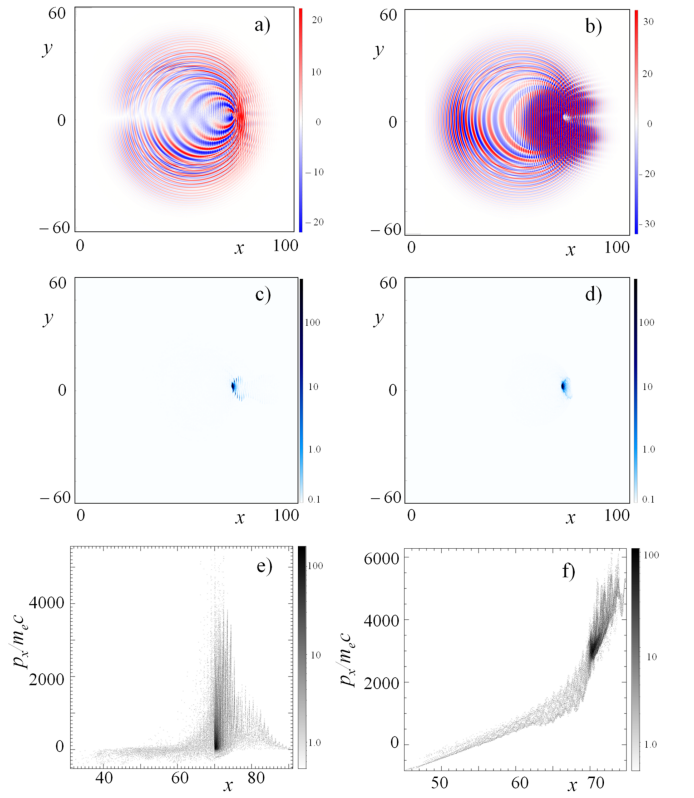


FIG. 4. a) and b) Distribution of the x - and z -components of the electric field; c) and d) of the electron and ion density in the (x, y) plane; e) and f) phase planes (x, p_x) of the electrons and ion ions, respectively, at $t = 100$. The initial off-axis displacement equals $\delta y = 0.25$.

is equal to 7×10^4 . The target has the form of an ellipsoid in the (x, y) plane with horizontal and vertical semi-axes equal to 1λ and 3.5λ . It is initially located at $x = 50\lambda$ in the near axis region with its y -coordinate varying from 0λ to 1.8λ . The target comprises of hydrogen plasma with proton-to-electron mass ratio equal to 1836. The electron density corresponds to the ratio $\omega_{pe}/\omega = 10$. A circularly polarized laser pulse is excited in the vacuum region at the left-hand side of the computation domain. The laser pulse has a Gaussian shape with a length of $l_x = 20\lambda$ and $l_y = 25\lambda$, and with dimensionless amplitude $a = eE/m_e\omega c$ varies from 250 to 325. Under the simulation conditions, the accelerated ion energy according to Eq. (20) is equal to 4.5 GeV. The acceleration length $l_{acc} = ct_{acc}$ is equal to 135λ .

The aim of the PIC simulations is to investigate the dependence of the energy of accelerated ions on the initial displacement of the target along the y -axis.

In Figs. 4 a) - d) we present electromagnetic field and electron and ion density distribution in the (x, y) plane at $t = 100$. Here and below the laser period $2\pi/\omega$ and wavelength λ are time and space units. Fig. 4 b), with the distribution of the z -component of the electromagnetic field in the (x, y) plane, shows the laser pulse reflection from the receding with relativistic velocity target. Due to the double Doppler effect the wavelength of the reflected light is substantially longer than the wavelength of the incident radiation. The laser field interaction with the plasma target is accompanied by the high order harmonics radiation distinctly seen in the short-wavelength scattered radiation. The up-down asymmetry of $E_x(x, y)$ appears due to asymmetry of the initial position of the target with respect to the laser pulse axis. There also it can be seen a strong longitudinal quasistatic (long wavelength) electric field formed at the rear side of the target. In this field the positively charged ion acceleration occurs. As it follows from Figs. 4 c) and d), where the electron and ion density distribution in the (x, y) plane is shown, the electrons pushed forward by the laser radiation move almost together with the ions pulled by the electric charge separation electric field. In Figs. e) and f) we present the phase planes (x, p_x) of the electrons and ion ions, respectively, which demonstrate that the highest energy electrons and ions are localised in the same region.

In the process of nonlinear interaction with the MLT the laser pulse becomes modulated in the transverse direction as we can see in Fig. 4 b). This makes the interaction with the target of initially Gaussian pulse to be similar to that of the super-Gaussian pulse. As a result, the dependences of the x - and y -components of the ion and electron momentum on the y -coordinate shown in Fig. 5 are in qualitative agreement with theoretical curves in Fig.3. Here it is possible to see a characteristic double maximum profile in the ion distribution in the (y, p_x) plane. The (y, p_y) distribution clearly shows

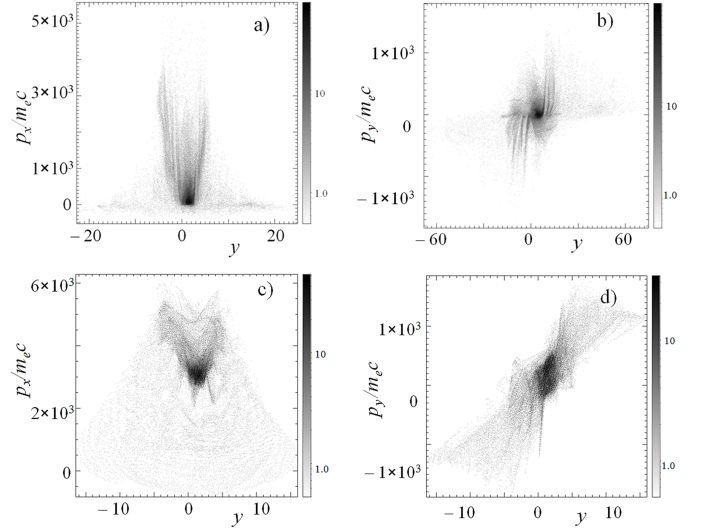


FIG. 5. a) and b) Electron phase planes (x, p_x) and (y, p_y) and c) and d) of the ions, at $t = 100$ for initial y coordinate equal to 0.25.

the target expansion at its periphery and the contraction in the near-axis region.

In Figs. 6 a), b), where we plot distribution of the electron and ion density in the (x, y) plane at $t = 250$, we see, although the target is strongly deformed and displaced in the vertical direction, the ions and electrons are mostly localized in the same region. The c) and d) frames present the phase planes (x, p_x) of the electrons and ion ions with the insets showing the electron and ion energy spectra, respectively. The electron component has a flat energy distribution with the maximum energy of the order of 8 GeV. The accelerated ion energy distribution shows a relatively narrow, approximately of 20%, peak at the energy of the order of 4 GeV. The ion phase plane (y, p_x) and ion phase plane (y, p_y) in Figs. 6 e) and f) demonstrate that the high energy ions remain localized in the near-axis region.

Dependence of the accelerated ion energy, \mathcal{E}_α , on the target initial position, δr_0 , is presented in Fig. 7 for different laser pulse amplitude. At the simulation conditions the accelerated ions reach their maximum energy at the time approximately equal to 250 fs, so all of the graphs are presented at that moment of time. Here we plot the theoretical curves (dashed lines) calculated by using Eqs. (40–42) and the energy value obtained in simulations (dots in color). The theoretical dependence of the ion energy on the initial target position follows from Eqs. (40) and (41). It reads

$$\mathcal{E}_{\alpha, \delta r_0} = m_\alpha c^2 \frac{2^{1/2}}{3} \frac{l_\perp^{3/4}}{c^{1/2} t_{1/3}^{1/2} \delta r_0^{1/4}}. \quad (56)$$

This expression is valid in the limit of substantially large δr_0 . When $\delta r_0 \rightarrow 0$ it formally tends to infinity. Ap-

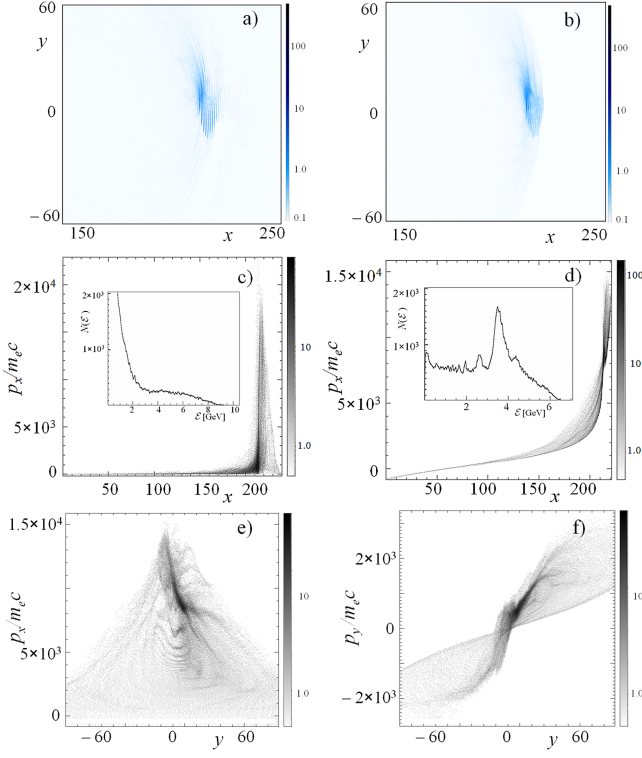


FIG. 6. a) and b) Distribution of the electron and ion density in the (x, y) plane; c) and d) phase planes (x, p_x) of the electrons and ion ions (the insets show the electron and ion energy spectra), respectively; e) ion phase plane (y, p_x) ; f) ion phase plane (y, p_y) , at $t = 250$ for initial y coordinate equal to 0.25.

parently, the ion energy from the off-axis localized target cannot be larger than the ion energy in the case of the target positioned exactly on the axis, $\mathcal{E}_{\alpha, max}$. In order to take this into account we shall use the interpolation formula

$$\frac{1}{\mathcal{E}_{\alpha}^s} = \frac{1}{\mathcal{E}_{\alpha, max}^s} + \frac{1}{\mathcal{E}_{\alpha, \delta r_0}^s} \quad (57)$$

with the fitting parameter $s \gg 1$. In the limit of small δr_0 the ion energy is equal to $\mathcal{E}_{\alpha, max}$. For large initial vertical coordinate it is proportional to $\delta r_0^{-1/4}$ according to Eq. (56). In Fig. 7 we plot the normalized ion energy γ_p achieved with the MLT initially shifted in the vertical direction versus the initial target coordinate δy_0 for different amplitudes of the Gaussian laser pulse. The plot markers are the 2D PIC simulation results and the curves correspond to theoretical dependences given by Eq. (57) for 1. $a = 325$; 2. $a = 300$; 3. $a = 275$; 4. $a = 250$).

For small the initial target coordinate the ion energy decreases with δy_0 more slowly than it is predicted by the theory due to self-modulation of the laser pulse in transverse direction, which is distinctly seen in the elec-

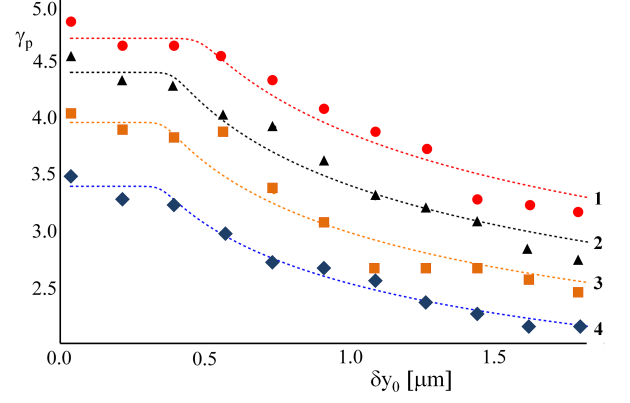


FIG. 7. Normalized proton energy gained with the MLT initially shifted in the vertical direction versus the initial target coordinate for different amplitudes of the Gaussian laser pulse (1. $a = 325$; 2. $a = 300$; 3. $a = 275$; 4. $a = 250$). The plot markers are the simulation results and the curves correspond to theoretical dependences.

tromagnetic field distribution in Fig. 4 b). The laser pulse self-modulation prevents the target from slepage out off the acceleration phase providing the fast ion collimation seen in Fig. 6 e). As it follows from dependences presented in Fig. 7, the laser pulse modulation effects are significant for $\delta y_0 < 0.5 \mu\text{m}$.

CONCLUSIONS AND DISCUSSIONS

We have studied the effects of the laser pulse transverse inhomogeneity on the ion acceleration in the RPDA regime. Within the framework of a thin foil approximation we found the dependence of the accelerated ion maximum energy on the off-axis displacement of the mass limited target for Gaussian and super-Gaussian laser pulse profiles. When the target is irradiated by the Gaussian laser pulse it is pushed away from the pulse by the ponderomotive pressure of electromagnetic radiation, while in the case super-Gaussian the central part of the target may undergo self-contraction provided its initial off-axis displacement is small enough. The 2D particle in cell simulations affirm the theoretical calculations at large initial coordinate of the target in the vertical direction, δy_0 . If the target is positioned in the vicinity of the axis, the self-modulation of the laser pulse in transverse direction prevents the target from slepage out off the acceleration phase providing the fast ion collimation.

The results obtained can be used for determining the required laser-target alignment parameters and/or diagnostics of the ion acceleration by the laser radiation pressure with mass limited targets, widely used in the experiments.

-
- * Also at the ITMO University, Saint-Petersburg 197101, Russia; Russian Acad. Sci., A. M. Prokhorov General Phys. Inst., Vavilov Str. 38, Moscow, 119991, Russia
- [1] M. Borghesi, J. Fuchs, S. V. Bulanov, A. J. Mackinnon, P. Patel, and M. Roth, *Fus. Sci. and Technology* **49**, 412 (2006)
 - [2] A. V. Korzhimanov, A. A. Gonoskov, E. A. Khazanov, and A. M. Sergeev, *Phys. Usp.* **54**, 9 (2011)
 - [3] H. Daido, M. Nishiuchi, and A. S. Pirozhkov, *Rep. Prog. Phys.* **75**, 056401 (2012)
 - [4] A. Macchi, M. Passoni, and M. Borghesi, *Rev. Mod. Phys.* **85**, 751 (2013)
 - [5] S. Yu. Gus'kov, *Plasma Phys. Rep.* **39**, 1 (2013)
 - [6] S. V. Bulanov, J. J. Wilkens, M. Molls, T. Zh. Esirkepov, G. Korn, G. Kraft, S. D. Kraft, and V. S. Khoroshkov, *Phys. Usp.* **57**, 1265 (2014)
 - [7] S. V. Bulanov, T. Zh. Esirkepov, M. Kando, J. Koga, K. Kondo, and G. Korn, *Plasma Phys. Rep.* **41**, 1 (2015)
 - [8] V. S. Beskin, *MHD Flows in Compact Astrophysical Objects*. (Springer, Berlin, 2010)
 - [9] E. V. Derishev, V. V. Kocharovsky, and V. V. Kocharovsky *ApJ*, **521**, 640 (1999)
 - [10] B. E. Stern and J. Poutanen, *MNRAS* **383**, 1695 (2008)
 - [11] D. Khangulyan, F. Aharonian, and V. Bosch-Ramon *MNRAS*, **383**, 467 (2008)
 - [12] B. Cerutti, A. Philippov, K. Parfrey, and A. Spitkovsky *MNRAS* (in press) <http://arxiv.org/abs/1410.3757>
 - [13] A. V. Gurevich, L. V. Pariskaya, and L. P. Pitaevskii, *Sov. Phys. JETP* **22**, 449 (1966)
 - [14] P. Mora, *Phys. Rev. Lett.* **90**, 185002 (2003)
 - [15] S. Wilks, W. L. Kruer, M. Tabak, and A. B. Langdon, *Phys. Rev. Lett.* **69**, 1383 (1992)
 - [16] S. P. Hatchett, C. G. Brown, T. E. Cowan, E. A. Henry, J. S. Johnson, M. H. Key, J. A. Koch, A. B. Langdon, B. F. Lasinski, R. W. Lee, A. J. Mackinnon, D. M. Pennington, M. D. Perry, T. W. Phillips, M. Roth, T. C. Sangster, M. S. Singh, R. A. Snavely, M. A. Stoyer, S. C. Wilks, and K. Yasuike, *Phys. Plasmas* **7**, 2076 (2000)
 - [17] I. Last, I. Schek, and J. Jortner, *J. Chem. Phys.* **107**, 6685 (1997)
 - [18] K. Nishihara, H. Amitani, M. Murakami, S. V. Bulanov, and T. Zh. Esirkepov, *Nucl. Instrum. Meth. Phys. Res. A* **464**, 98 (2001)
 - [19] V. F. Kovalev and V. Yu. Bychenkov, *Phys. Rev. Lett.* **90**, 185004 (2003)
 - [20] M. Murakami and M. M. Basko, *Phys. Plasmas* **13**, 012105 (2006)
 - [21] V. I. Veksler, *At. Energ.* **2**, 427 (1957)
 - [22] T. Zh. Esirkepov, M. Borghesi, S. V. Bulanov, G. Mourou, and T. Tajima, *Phys. Rev. Lett.* **92**, 175003 (2004)
 - [23] O. Klimo, J. Psikal, J. Limpouch, and V. T. Tikhonchuk, *Phys. Rev. ST Accel. Beams* **11**, 031301 (2008)
 - [24] A. P. L. Robinson, M. Zepf, S. Kar, R. G. Evans, and C. Bellei, *New J. Phys.* **10**, 013021 (2008)
 - [25] A. V. Vshivkov, N. M. Naumova, F. Pegoraro, and S. V. Bulanov, *Phys. Plasmas* **5**, 2752 (1998)
 - [26] S. V. Bulanov, T. Zh. Esirkepov, M. Kando, S. S. Bulanov, S. G. Rykovanov, and F. Pegoraro, *Phys. Plasmas* **20**, 123114 (2013)
 - [27] S. S. Bulanov, C. B. Schroeder, E. Esarey, and W. P. Leemans, *Phys. Plasmas* **19**, 093112 (2012)
 - [28] S. V. Bulanov, T. Zh. Esirkepov, M. Kando, A. S. Pirozhkov, N. N. Rosanov, *Phys. Usp.* **56**, 429 (2013)
 - [29] S. Kar, M. Borghesi, S. V. Bulanov, A. Macchi, M. H. Key, T. V. Liseykina, A. J. Mackinnon, P. K. Patel, L. Romagnani, A. Schiavi, and O. Willi, *Phys. Rev. Lett.* **100**, 225004 (2008)
 - [30] A. Henig, S. Steinke, M. Schnuerer, T. Sokollik, R. Hoyerlein, D. Kiefer, D. Jung, J. Schreiber, B. M. Hegelich, X. Q. Yan, J. Meyer-ter-Vehn, T. Tajima, P. V. Nickles, W. Sandner, and D. Habs, *Phys. Rev. Lett.* **103**, 245003 (2009)
 - [31] S. Kar, K. F. Kakolee, B. Qiao, A. Macchi, M. Cerchez, D. Doria, M. Geissler, P. McKenna, D. Neely, J. Osterholz, R. Prasad, K. Quinn, B. Ramakrishna, G. Sarri, O. Willi, X. Y. Yuan, M. Zepf, and M. Borghesi, *Phys. Rev. Lett.* **109**, 185006 (2012)
 - [32] J. Limpouch, J. Psikal, A. A. Andreev, K. Yu. Platonov, and S. Kawata, *Laser and Particle Beams* **26**, 225 (2008)
 - [33] A. A. Andreev, J. Limpouch, J. Psikal, K. Yu. Platonov, and V. T. Tikhonchuk, *Eur. Phys. J. ST* **175**, 123 (2009)
 - [34] T. Kluge, W. Enghardt, S. D. Kraft, U. Schramm, K. Zeil, T. E. Cowan and M. Bussmann, *Phys. Plasmas* **17**, 123103 (2010)
 - [35] K. Zeil, J. Metzkes, T. Kluge, M. Bussmann, T. E. Cowan, S. D. Kraft, R. Sauerbrey, B. Schmidt, M. Zier, and U. Schramm, *Plasma Phys. Control. Fusion* **56**, 084004 (2014)
 - [36] A. Zigler, S. Eisenman, M. Botton, E. Nahum, E. Schleifer, A. Baspaly, I. Pomerantz, F. Abicht, J. Branzel, G. Priebe, S. Steinke, A. Andreev, M. Schnuerer, W. Sandner, D. Gordon, P. Sprangle, and K. W. D. Ledingham, *Phys. Rev. Lett.* **110**, 215004 (2013)
 - [37] J. W. Wang, M. Murakami, S. M. Weng, H. Xu, J. J. Ju, S. X. Luan, and W. Yu, *Phys. Plasmas* **21**, 123103 (2014).
 - [38] T. P. Yu, Z. M. Sheng, Y. Yin, H. B. Zhuo, Y. Y. Ma, F. Q. Shao and A. Pukhov *Phys. Plasmas* **21**, 053105 (2014)
 - [39] Y. Fukuda, A. Ya. Faenov, M. Tampo, T. A. Pikuz, T. Nakamura, M. Kando, Y. Hayashi, A. Yogo, H. Sakaki, T. Kameshima, A. S. Pirozhkov, K. Ogura, M. Mori, T. Zh. Esirkepov, J. Koga, A. S. Boldarev, V. A. Gasilov, A. I. Magunov, T. Yamauchi, R. Kodama, P. R. Bolton, Y. Kato, T. Tajima, H. Daido, and S. V. Bulanov, *Phys. Rev. Lett.* **103**, 165002 (2009)
 - [40] T.-P. Yu, A. M. Pukhov, Z.-M. Sheng, F. Liu, and G. Shvets, *Phys. Rev. Lett.* **110**, 045001 (2013)
 - [41] S. V. Bulanov, E. Yu. Echkina, T. Zh. Esirkepov, I. N. Inovenkov, M. Kando, F. Pegoraro, and G. Korn, *Phys. Rev. Lett.* **104**, 135003 (2010)
 - [42] S. V. Bulanov, E. Yu. Echkina, T. Zh. Esirkepov, I. N. Inovenkov, M. Kando, F. Pegoraro, and G. Korn, *Phys. Plasmas* **17**, 063102 (2010)
 - [43] F. Pegoraro and S. V. Bulanov, *Phys. Rev. Lett.* **99**, 065002 (2007)
 - [44] T. Zh. Esirkepov, *Comput. Phys. Commun.* **135**, 144 (2001)
 - [45] E. Ott, *Phys. Rev. Lett.* **29**, 142 (1972)
 - [46] W. Manheimer, D. Colombait, and E. Ott, *Phys. Fluids* **27**, 2164 (1984)
 - [47] T. Taguchi and K. Mima, *Phys. Plasmas* **2**, 2790 (1995)
 - [48] G. A. Korn and T. M. Korn, *Mathematical Handbook for Scientists and Engineers*. (Dover Publ., New York, 2000)
 - [49] E. Yu. Echkina, I. N. Inovenkov, T. Zh. Esirkepov, F.

- Pegoraro, M. Borghesi, and S. V. Bulanov, *Plasma Phys. Rep.* **36**, 15 (2010)
- [50] S. V. Bulanov, T. Zh. Esirkepov, M. Kando, F. Pegoraro, S. S. Bulanov, C. G. R. Geddes, C. B. Schroeder, E. Esarey, and W. P. Leemans, *Phys. Plasmas* **19**, 103105 (2012)
- [51] A. Macchi, S. Veghini, and F. Pegoraro, *Phys. Rev. Lett.* **103**, 085003 (2009)
- [52] S. Humphries, Jr., *Principles of Charged Particle Acceleration* (Wiley, New York, 1999)